



# Hybrid Plasmon Modes at Chiroferrite-Graphene Interface

M. Umair<sup>1</sup> · A. Ghaffar<sup>1</sup> · F. Razzaz<sup>2,3</sup> · S. M. Saeed<sup>2</sup>

Received: 5 October 2023 / Accepted: 27 November 2023 / Published online: 8 December 2023  
© The Author(s), under exclusive licence to Springer Science+Business Media, LLC, part of Springer Nature 2023

## Abstract

In this paper, numerical investigations are carried out to explore the characteristics of hybrid plasmon modes at chiroferrite-graphene interface. Kubo formula is utilized for the modeling of monolayer graphene conductivity, and the impedance boundary condition approach is applied at the chiroferrite-graphene interface to obtain the dispersion relation. Frequency dependent normalized propagation constant under the different values of graphene's chemical potential ( $\mu$ ), relaxation time ( $\tau$ ), number of graphene layers ( $N$ ), temperature ( $T$ ), and constitutive parameter of chiroferrite medium such as chirality and gyrotropy are analyzed. Control on graphene and chiroferrite parameters may be useful for chiral sensing, microwave devices, antennas, and magnetic resonance imaging in the terahertz (THz) frequency band.

**Keywords** Chiroferrite · Graphene · Plasmon · Characteristics equation

## Introduction

Data transmission systems increasingly rely on photonic devices due to rapid technological advancements in optical techniques. In the future, reducing the element size will be expected to allow for 10 Tbits/s/1 of data transmission by reducing the size of nanophotonic devices to nanometer; in this way, data storage will be up to 1Tbit per inch. Because Abbe's diffraction limit reaches approximately one-half of the optical wavelength, it is extremely difficult to reduce the element sizes to nanometers in conventional photonic devices. A promising method of controlling propagation and dispersion of light on the nanometer scale is through excitation of surface plasmon polaritons (SPPs) that

can defeat the diffraction limit [1]. SPPs are a special kind of electromagnetic waves existing between metal and dielectric interface [2–7]. So far, numerous plasmonic components based on metal have been studied [8–11]. However, metal-based plasmonic structures have been hindered by higher intrinsic losses, low mode of confinement, and poor tenability [12]. In the last few years, graphene has gained much attention due to its excellent optical and electronic properties, providing compact, strong mode confinement, low propagation loss, and tunable components. Due to their superior tuning and compactness, graphene is considered a superb candidate for use in next-generation nano-plasmonic chips and optical devices. Additionally, these features can be tailored by tailoring graphene conductivity [13]. Numerous graphene-based devices have been proposed, including bends, splitters, optical waveguides, metasurface absorbers, logic gates, lenses, filters, switches, and directional couplers [14]. Guangcan Mi and Vien Van analyzed the analyze the numerical calculation of EM wave at chiral-metal interface for on-chip chiral sensing and enantiomer detection application [15]. M Z Yaqoob presented theoretical analysis of planar structure at chiral-graphene interface for chiral sensing applications [16]. Further control on plasmon chiroferrite-graphene planar structure is analyzed which is not presented yet.

It was discovered in the nineteenth century that some biological or crystalline materials exhibited optical activity, and by the middle of the century, it was hypothesized that this phenomenon was attributed to the chirality of their molecules. Several studies have been conducted on electromagnetic propagation in

✉ A. Ghaffar  
aghaffar16@uaf.edu.pk  
M. Umair  
rumair.uaf@gmail.com  
F. Razzaz  
f.kasim@psau.edu.sa  
S. M. Saeed  
s.saeed@psau.edu.sa

<sup>1</sup> Department of Physics, University of Agriculture, 38000 Faisalabad, Pakistan  
<sup>2</sup> Electrical Engineering Department, College of Engineering, Prince Sattam Bin Abdulaziz University, 16278, Al-Kharj, Saudi Arabia  
<sup>3</sup> Faculty of Engineering and Information Technology, Taiz University, 6803 Taiz, Yemen

chiral materials. Chiral medium can rotate the plane of polarization of an electromagnetic wave to the right or left depending on its handedness. Creating an isotropic chiral material allows very limited control over its chirality. The development of methods to achieve chirality control is therefore of utmost importance. This can be accomplished by introducing specific types of anisotropy. A chiral medium and a nonreciprocal ferrite medium can be combined to form a composite chiroferrite medium by immersing chiral objects in a magnetically biased ferrite whose permeability is gyrotropic. By modifying the biased static magnetic field, one can control gyrotropy of the permeability and thus control the chirality within the waveguide. The longitudinal components and eigenmode solution of this electromagnetic problem are complex in chiroferrite media due to the intrinsic coupling between electric and magnetic fields [17]. Chiroferrite materials can be used to control the radiation properties of printed circuit antennas. Additionally, chiroferrite material has numerous applications in optical communication and integrated optics. In this manuscript, hybrid plasmon modes are studied at chiroferrite-graphene planar interface. Frequency-dependent normalized propagation constant for various values of chemical potential, relaxation time, number of graphene layers, temperature, chirality, and gyrotropy are analyzed. The presented research may be useful for chiral sensing, microwave devices, antennas, and magnetic resonance imaging in the terahertz (THz) frequency band.

### Methodology

The analytical formulation of chiroferrite-graphene has been presented in this section. SPP wave is propagating in z axis as shown in Fig. 1.

Constitutive relations for chiroferrite material [18] as follow:

$$D = \epsilon E + i\xi B \tag{1}$$

$$H = i\xi E + \bar{\mu}^{-1} B \tag{2}$$

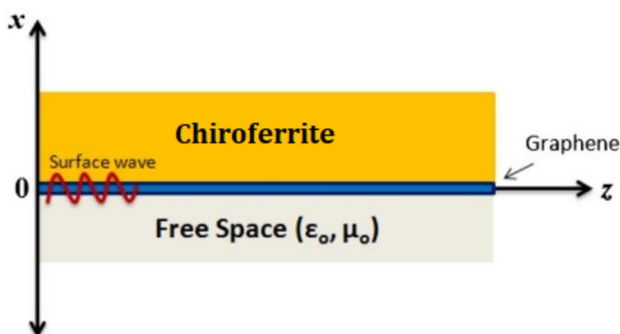


Fig. 1 Geometry for chiroferrite-graphene interface

$\epsilon$  and  $\xi$  represent the permittivity and chirality respectively of chiroferrite medium.  $\bar{\mu}^{-1}$  represents permeability tensor as reported in [18].

$$\bar{\mu} = \begin{pmatrix} \mu_1 & -ik & 0 \\ ik & \mu_1 & 0 \\ 0 & 0 & \mu_3 \end{pmatrix} \tag{3}$$

The EM field components for chiroferrite medium are:

$$E_z = A_1 e^{-q_1 x} + A_2 e^{-q_2 x} \tag{4}$$

$$H_z = i(A_1 \alpha_1 e^{-q_1 x} + A_2 \alpha_2 e^{-q_2 x}) \tag{5}$$

Remaining EM fields components for chiroferrite medium can be derived from [19].

$$E_x = -ie^{-i-x(q_1+q_2)}(A_1 q_1 e^{q_2 x}(a + c\alpha_1) + A_2 q_2 e^{q_1 x}(a + c\alpha_2)) \tag{6}$$

$$E_y = e^{-i-x(q_1+q_2)}(A_1 q_1 e^{q_2 x}(b - d\alpha_1) + A_2 q_2 e^{q_1 x}(b - d\alpha_2)) \tag{7}$$

$$H_x = e^{-i-x(q_1+q_2)}(-A_1 q_1 e^{q_2 x}(e - a\alpha_1) - A_2 q_2 e^{q_1 x}(e - a\alpha_2)) \tag{8}$$

$$H_y = ie^{-i-x(q_1+q_2)}(A_1 q_1 e^{q_2 x}(f + b\alpha_1) + A_2 q_2 e^{q_1 x}(f + b\alpha_2)) \tag{9}$$

Following are coupled wave equations obtained from the source-free Maxwell equations.

$$\nabla_t^2 E_z + P_1 E_z + iP_2 H_z = 0 \tag{10}$$

$$\nabla_t^2 H_z + iP_3 E_z + P_4 H_z = 0 \tag{11}$$

The EM wave coefficients of 6 and 7 are given below.

$$P_1 = \frac{\omega(d(\epsilon_0 + \mu_z \xi^2) - \mu_z \xi b)}{D_2} \tag{12}$$

$$P_2 = \frac{\omega \mu_z (b - d\xi)}{D_2} \tag{13}$$

$$P_3 = \frac{\omega(b(\epsilon_0 + \mu_z \xi^2) + f \mu_z \xi)}{D_2} \tag{14}$$

$$P_4 = \frac{\omega \mu_z (b\xi + f)}{D_2} \tag{15}$$

where,

$$a = [\beta^3 + 3\omega k \xi \beta^2 + 2\omega^2 \xi^2 \beta (\mu_1^2 - k^2) + \omega^2 \mu_1 \epsilon_0 \beta] / D_1 \tag{16}$$

$$b = [\omega\beta(\mu_1\xi\beta + \omega\varepsilon_0k) + \omega^3\varepsilon_0\xi(\mu_1^2 - k^2)]/D_1 \tag{17}$$

$$c = [2\omega^2\xi\beta(\mu_1^2 - k^2) + \omega k\beta^2]/D_1 \tag{18}$$

$$d = [-\omega\mu_1\beta^2 - \omega^3\varepsilon_0(\mu_1^2 - k^2)]/D_1 \tag{19}$$

$$e = -\omega[\xi\beta(2\omega\varepsilon_0\mu_1 + \xi k\beta) + 2\omega\xi^3\beta(\mu_1^2 - k^2) + \omega^2\varepsilon_0^2k]/D_1 \tag{20}$$

$$f = \left[ \omega\beta^2(\varepsilon_0 + \mu_1\xi^2) - 2\omega^2\varepsilon_0\xi c\beta k - \omega^3\xi c^2\varepsilon_0(\mu_1^2 - k^2) - \omega^3\varepsilon_0^2\mu_1 \right] / D_1 \tag{21}$$

$$D_1 = \beta^4 + 4\omega^2\xi^2\beta^2(k^2 - \mu_1^2) - 2\omega^2\beta^2\mu_1\varepsilon_0 + \omega^4\varepsilon_0^2(\mu_1^2 - k^2) - 4\omega\xi\beta^3k \tag{22}$$

$$D_2 = b^2 + df \tag{23}$$

$$q_1 = \sqrt{\frac{P_1 + P_4 + \sqrt{(P_1 - P_4)^2 - 4P_2P_3}}{2}} \tag{24}$$

$$q_2 = \sqrt{\frac{P_1 + P_4 - \sqrt{(P_1 - P_4)^2 - 4P_2P_3}}{2}} \tag{25}$$

$$\alpha_1 = \frac{P_1 - (q_1)^2}{P_2} \tag{26}$$

$$\alpha_2 = \frac{P_1 - (q_2)^2}{P_2} \tag{27}$$

Electromagnetic field components for free space are given below:

$$E_z = A_3e^{amx} \tag{28}$$

$$H_z = A_4e^{amx} \tag{29}$$

Here,  $am = \sqrt{\beta^2 - \omega^2\varepsilon_0\mu_0}$ . The remaining EM field components can be derived from [16]. Following boundary conditions to be enforced at chiroferrite-graphene interface.

$$\hat{x} \times [H_1 - H_2] = \sigma E \tag{30}$$

$$\hat{x} \times [E_1 - E_2] = 0 \tag{31}$$

$\sigma$  is the conductivity of monolayer graphene as follows:

$$\begin{aligned} \sigma(\mu, \tau, T) &= \frac{ie^2(\omega - j\tau^{-1})}{\pi\hbar^2} \\ &\times \left[ \frac{1}{(\omega - i\tau^{-1})^2} \int_0^\infty \right. \\ &\times \xi_{en} \left( \frac{\sigma f_d(\xi_{en}, \mu, T)}{\sigma\xi} - \frac{\sigma f_d(-\xi_{en}, \mu, T)}{\sigma\xi} \right) d\xi_{en} \\ &\left. - \int_0^\infty \times \frac{f_d(-\xi_{en}, \mu, T) - f_d(\xi_{en}, \mu, T)}{(\omega - i\tau^{-1})^2 - 4\left(\frac{\xi}{\hbar}\right)^2} d\xi_{en} \right] \end{aligned} \tag{32}$$

where  $\mu$  is chemical potential,  $\tau$  is relaxation rate, T is temperature,  $e$ , charge on electron,  $f_d$  is Fermi–Dirac,  $\omega$  is operating frequency,  $\xi_{en}$ , energy, and  $\hbar$  represent the reduced Plank’s constant [20]. By applying boundary conditions, the following dispersion relation is obtain.

$$\begin{aligned} am(\omega q_1(f + b\alpha_1)\alpha_2\mu_0 - \omega q_2\alpha_1(f + b\alpha_2)\mu_0 \\ - (b^2 + df)q_1q_2(-\alpha_1 + \alpha_2)(am - i\sigma\omega\mu_0)) \\ - (iam\sigma + \varepsilon_0\omega)(\omega(\alpha_1 - \alpha_2)\mu_0 + q_1(b - d\alpha_1) \\ (am - i\sigma\omega\mu_0) - q_2(b - d\alpha_2)(am - i\sigma\omega\mu_0)) = 0 \end{aligned} \tag{33}$$

### Results and Discussion

This section presents the analytical results to explore the characteristics of hybrid plasmon modes at chiroferrite-graphene planar structure. In all graphs, the chemical potential of monolayer graphene is set to be  $\mu = 0.1eV$ , relaxation time  $\tau = 20 \times 10^{-13}s$ , temperature  $T = 300K$ , chirality  $\xi = 0.002$ , and gyrotropy of ferrite medium  $k = 0.6\mu_0$ . Characteristic curve analysis is utilized to study the behavior of electromagnetic surface waves on graphene planar interface loaded with semi-infinite chiroferrite medium. Normalized propagation constant  $Re(\frac{\beta}{k_0})$  is a powerful parameter for designing the plasmonic devices, which shows the factor of confinement in the plasmonic structure.  $\beta$  represents propagation constant and  $k_0 = \sqrt{\omega^2\varepsilon_0\mu_0}$ . Two propagating modes (upper and lower) appeared.

due to the existence of chiroferrite medium. Frequency dependent normalized propagation constant under the different graphene features, chirality, and gyrotropy of the ferrite medium are studied. Since graphene supports THz frequencies [13, 17–22], numerical results are taken in THz frequency range. To study the factor of confinement, which is a very crucial parameter for the practical point of view to fabricate nanophotonic devices, it is analyzed in Fig. 2a for three various values of chemical potential.

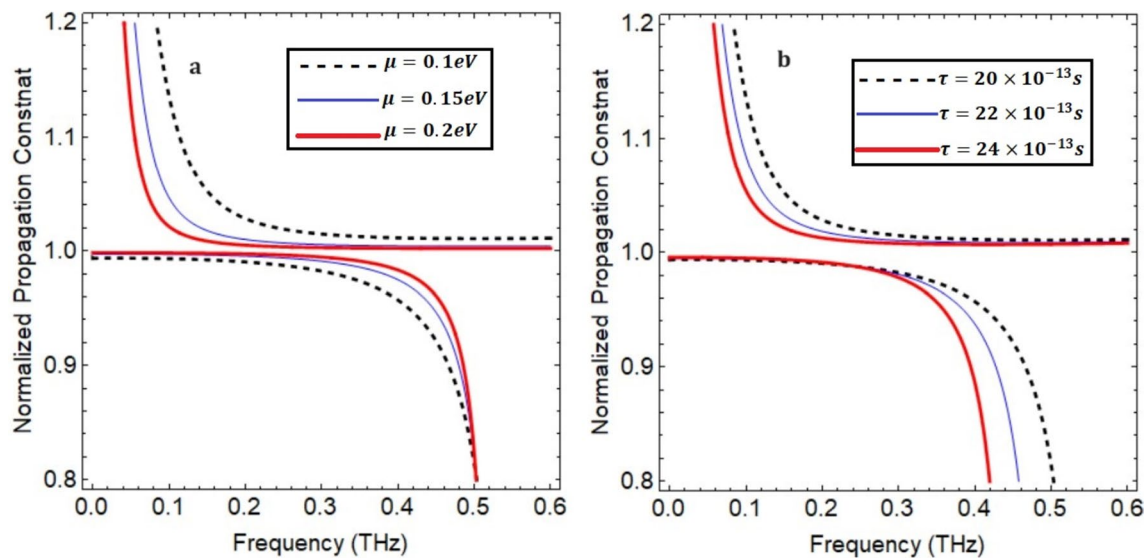


**Fig. 2** Influence of chemical potential and relaxation time on normalized propagation constant

The upper mode shows greater variation in characteristic curves as compared to lower mode. Characteristic curves for both modes start squeezing for higher magnitude of chemical potential. For the case of the upper mode, normalized propagation starts decreasing by increasing of chemical potential as reported [16, 21–23] and characteristic curves start shifting toward low frequency region as reported in [16]. The slope of variation of characteristic curve is greater for smaller value of chemical potential as reported in [22]. It can be noted that the frequency band for both modes can be tuned by varying chemical potential. Furthermore, lower mode shows a smaller variation in band gap as compared to the upper mode. As the chemical potential rises, the propagation constant decreases. This can be understood by considering the behavior of the energy bands in graphene. At low carrier concentrations, the valence and conduction bands in graphene meet at a single point in the Brillouin zone, known as the Dirac point. At this point, the energy–momentum relation for electrons becomes linear, leading to unique electronic properties. However, as chemical potential increases, electron density also increases, the energy bands shift, and the Dirac point moves away from the zero-energy level. At this point, the energy–momentum relation for electrons becomes linear, leading to unique electronic properties. However, as chemical potential increases, electron density also increases, the energy bands shift, and the Dirac point moves away from the zero-energy level. In other words, at higher electron densities (higher chemical potentials), the plasmons experience more damping, causing them to lose their energy faster and leading to a shorter propagation for the electromagnetic wave.

At this point, the energy–momentum relation for electrons becomes linear, leading to unique electronic properties. However, as chemical potential increases, electron density also increases, the energy bands shift, and the Dirac point moves away from the zero-energy level. In other words, at higher electron densities (higher chemical potentials), the plasmons experience more damping, causing them to lose their energy faster and leading to a shorter propagation for the electromagnetic wave. Therefore, there is a trade-off for choosing a suitable chemical potential to achieve the desired values of normalized propagation constant. The variation in Frequency dependent normalized propagation constant under the different values of relaxation time is depicted in Fig. 2b. As relaxation time increases, the characteristic curves for both modes start moving toward a low-frequency region. The bandgap between the upper and lower modes starts squeezing as the relaxation time increases; this confirms that electromagnetic surface.

waves are strongly dependent on the quality and traits of monolayer graphene layer. In the respect that normalized propagation increases with decreasing relaxation time, the variation of upper mode is almost the same, like in the chemical potential case, but the difference lies in their lower modes. Furthermore, the slope of variation of characteristic curve is greater for smaller value of relaxation time. It can be noted that, as relaxation time increases, normalized propagation starts decreasing as reported in [24, 25], and characteristic curves starts shifting towards low-frequency region. Furthermore, the lower mode becomes more dominant as compared to the higher mode. By optimizing relaxation time, it is possible to enhance the performance and reliability of nanophotonic devices. As the relaxation time

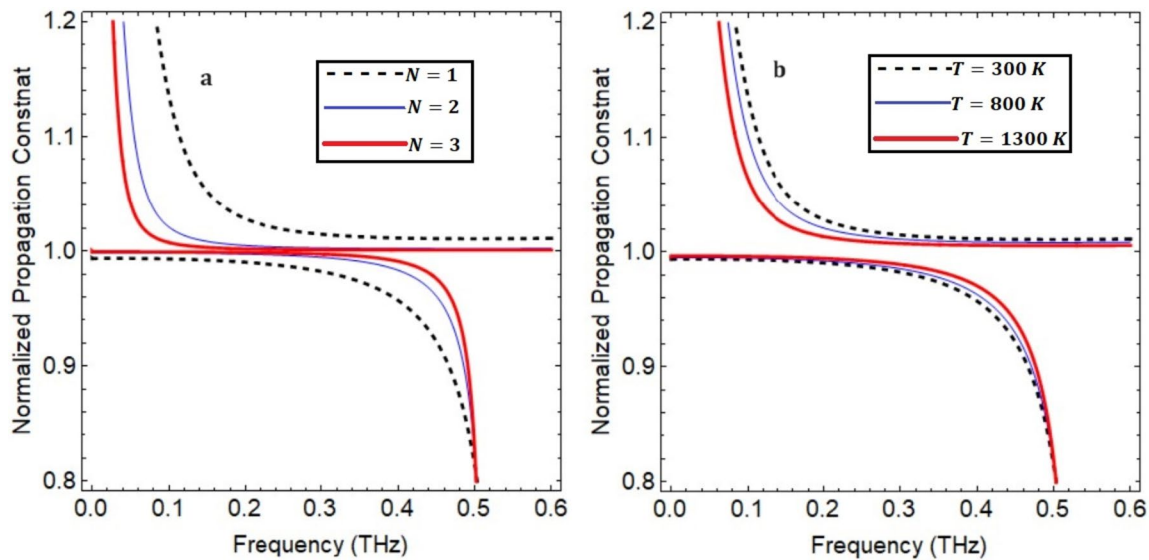


**Fig. 3** Influence of number of graphene layers and temperature on normalized propagation constant

increases, the scattering of electrons by phonons becomes more frequent and prominent. These scattering events cause the electrons to lose energy and momentum, resulting in a decrease in the propagation constant. Furthermore, the scattering process leads to a decrease in the overall conductivity of graphene and affects the propagation of electromagnetic waves in the material. Figure 3a analyzes the influence of the number of graphene layers on the normalized propagation constant since a monolayer of graphene absorbs only 2.3% of incident light as reported in [24, 26]. For the case of the upper mode, as number of graphene layers increases, normalized propagation constant starts decreasing as reported in [24, 25, 27]. The slope variation is greater for monolayer graphene as compared to multilayers. For the case of the upper mode, by increasing number of graphene layers the EM wave frequency decreases and characteristic curves exhibit smaller variation. After some higher frequencies, an unphysical region starts that has no practical importance in the plasmonics community. Additionally, the monolayer graphene exhibits higher variation characteristic curves. For the case of the lower mode, the variation in characteristic curves is shown at some higher frequencies. To demonstrate the influence of temperature on the normalized propagation constant, it is depicted in Fig. 3b. For the case of the upper mode, higher propagation constant could be achieved for lower temperature values. For the case of the lower mode, characteristic curves show very small variation in characteristic curves. The decrease in the normalized propagation constant with increasing temperature of graphene conductivity can be attributed to the increased scattering of electrons due to thermal energy and the enhanced electron–phonon interactions. These factors disrupt electron

motion and reduce the overall conductivity of graphene. It is concluded that as temperature rises, normalized propagation constant starts decreasing for the upper mode and vice versa for the lower mode, as shown in Fig. 3a. But the difference lies in their frequency band gap. Frequency dependent normalized propagation constant of under the different values of chirality parameter is analyzed in Fig. 4a. It is worth mentioning that as the chirality parameter increases, the normalized propagation constant starts increasing as reported in [18]. Lower mode characteristic curves begin to level off at lower frequencies while the upper mode at higher frequencies has practical importance. In optics, chiral materials can be used to manipulate the propagation of light in unique ways. By controlling the chirality of a material, researchers can effectively control the speed at which light propagates through it, leading to applications such as chiral optics and chiral metamaterials. Frequency dependent normalized propagation constant for the various values of gyrotropy (permeability tensor parameter) in certain THz frequency band is illustrated in Fig. 4b. The upper mode shows higher variation in characteristic curves as compared to lower mode. By increasing gyrotropy, the frequency band starts squeezing, and characteristic curves are shifted from low-frequency to high-frequency region. It is noted that from the above discussion, gyrotropy and chirality show the same trend for normalized propagation constant, but the difference lies in their frequency band gap. Furthermore, for the case of gyrotropy, lower mode characteristic curves level off at 0.51 THz. As the wave interacts with the gyrotropic medium, its velocity changes, affecting the rate at which it propagates through the material. The rotation of the polarization plane reduces losses and allows for a more efficient

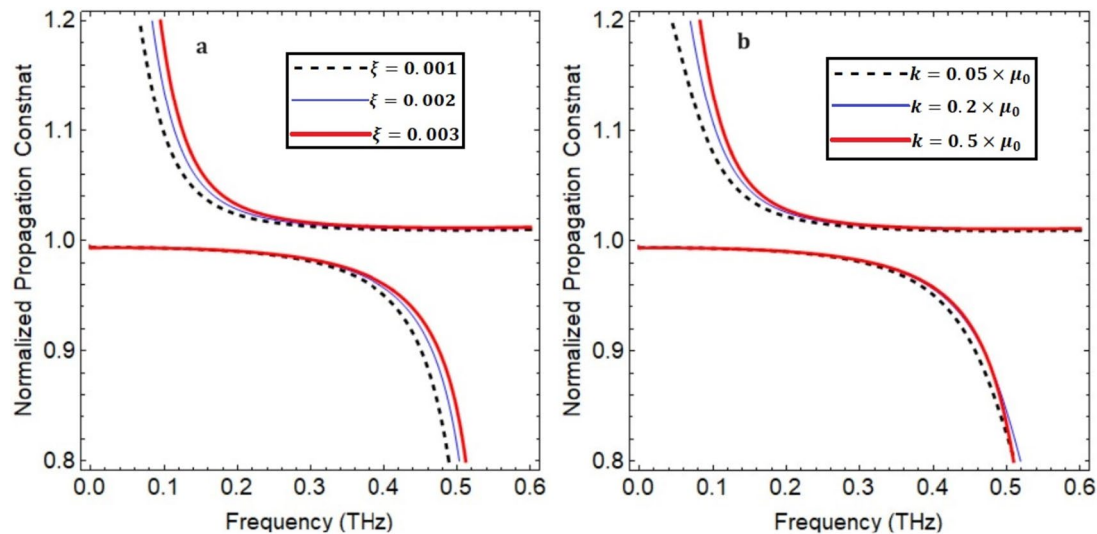


**Fig. 4** Influence of chirality and gyrotropy on normalized propagation constant

interaction between the wave and the material. Additionally, the alteration of the refractive index contributes to a higher propagation speed. These combined effects make ferrite mediums with increased gyrotropy particularly useful in applications such as microwave devices, antennas, and magnetic resonance imaging. This is an important matter for designing chiroferrite-graphene-based nanophotonic devices in the specific frequency band by choosing the appropriate gyrotropy of medium.

## Conclusion

Theoretical investigations were carried out to explore hybrid plasmon modes at the chiroferrite-graphene interface. Maxwell's equations in differential form were used to find the model field equations, and impedance boundary conditions were applied to obtain dispersion relation. Frequency dependence normalized propagation constant under the different values of graphene chemical potential, relaxation, number of graphene layers, temperature, chirality, and gyrotropy of the chiroferrite medium were analyzed. It is concluded that normalized propagation constant can be tailored by tailoring the abovementioned parameters to fabricate nanophotonic devices in THz frequency range.

**Authors' Contributions** M. Umair wrote main manuscript and derived analytical expressions. A. Ghaffar edited the manuscript and reviewed the numerical analysis. F. Razzaz and S. M. Saeed developed methodology in the given study. Author M. Umair was also encouraged and completely supervised during the preparation of the manuscript by A. Ghaffar. All authors reviewed the manuscript before submission.

**Funding** Prince Sattam bin Abdulaziz University, PSAU/2023/R/1444.

**Availability of Data and Materials** Detail about data has been provided in the article.

## Compliance with Ethical Standards

**Ethics Approval** Not applicable.

**Human and Animal Rights and Informed Consent** This article does not contain any studies with human or animal subjects performed by any of the authors.

**Conflict of Interest** The authors declare that they have no known competing financial interests or personal relationships that could have appeared to influence the work reported in this paper.

## References

1. Zhang J, Zhang L, Xu W (2012) Surface plasmon polaritons: physics and applications. *J Phys D Appl Phys* 45(11):113001
2. Krenn J, Weeber J-C (2004) Surface plasmon polaritons in metal stripes and wires. *Philosophical transactions of the royal society of London. Series A Math Phys Eng Sci* 362(1817):739–756
3. Liu W-C, Tsai DP (2002) Optical tunneling effect of surface plasmon polaritons and localized surface plasmon resonance. *Phys Rev B* 65(15):155423
4. Pitarke J et al (2006) Theory of surface plasmons and surface-plasmon polaritons. *Rep Prog Phys* 70(1):1
5. Saxler J et al (2004) Time-domain measurements of surface plasmon polaritons in the terahertz frequency range. *Phys Rev B* 69(15):155427
6. Törmä P, Barnes WL (2014) Strong coupling between surface plasmon polaritons and emitters: a review. *Rep Prog Phys* 78(1):013901
7. Zayats AV, Smolyaninov II, Maradudin AA (2005) Nano-optics of surface plasmon polaritons. *Phys Rep* 408(3–4):131–314

8. Dolatabady A, Granpayeh N (2015) L-shaped filter, mode separator and power divider based on plasmonic waveguides with nanocavity resonators. *IET Optoelectron* 9(6):289–293
9. Dolatabady A, Granpayeh N (2017) All-optical logic gates in plasmonic metal–insulator–metal nanowaveguide with slot cavity resonator. *J Nanophotonics* 11(2):026001–026001
10. Hu F, Yi H, Zhou Z (2011) Band-pass plasmonic slot filter with band selection and spectrally splitting capabilities. *Opt Express* 19(6):4848–4855
11. Lu H et al (2011) Ultrafast all-optical switching in nanoplasmonic waveguide with Kerr nonlinear resonator. *Opt Express* 19(4):2910–2915
12. Grigorenko AN, Polini M, Novoselov K (2012) Graphene plasmonics. *Nat Photonics* 6(11):749–758
13. Zhao T et al (2016) Plasmon modes of circular cylindrical double-layer graphene. *Opt Express* 24(18):20461–20471
14. Asgari S, Dolatabady A, Granpayeh N (2017) Tunable midinfrared wavelength selective structures based on resonator with antisymmetric parallel graphene pair. *Opt Eng* 56(6):067102–067102
15. Mi G, Van V (2014) Characteristics of surface plasmon polaritons at a chiral–metal interface. *Opt Lett* 39(7):2028–2031
16. Yaqoob MZ et al (2019) Characteristics of light–plasmon coupling on chiral–graphene interface. *JOSA B* 36(1):90–95
17. Xu J et al (2009) Electromagnetic wave propagation in an elliptical chiroferrite waveguide. *J Electromag Waves Appl* 23(14–15):2021–2030
18. Xu J-P (1996) Propagation characteristics of a circular waveguide filled with a chiroferrite medium. *Int J Infrared Millimeter Waves* 17:193–203
19. Gong J (1999) Electromagnetic wave propagation in a chiroplasma-filled waveguide. *J Plasma Phys* 62(1):87–94
20. Falkovsky L, Varlamov A (2007) Space-time dispersion of graphene conductivity. *The European Physical Journal B* 56:281–284
21. Gric T (2019) Tunable terahertz structure based on graphene hyperbolic metamaterials. *Opt Quant Electron* 51(6):202
22. Heydari MB, Samiei MHV (2021) TM-polarized surface plasmon polaritons in nonlinear multi-layer graphene-based waveguides: an analytical study. *arXiv preprint* <http://arxiv.org/abs/2101.02536>
23. Gric T, Hess O (2017) Tunable surface waves at the interface separating different graphene-dielectric composite hyperbolic metamaterials. *Opt Express* 25(10):11466–11476
24. Azam M et al (2021) Dispersion characteristics of surface plasmon polaritons (SPPs) in graphene–chiral–graphene waveguide. *Waves Random Complex Media* 1–12
25. Umair M et al (2020) Characteristics of surface plasmon polaritons in magnetized plasma film walled by two graphene layers. *J Nanoelectron Optoelectron* 15(5):574–579
26. Saeed M et al (2022) Graphene-based plasmonic waveguides: a mini review. *Plasmonics* 17(3):901–911
27. Shahid MU et al (2023) Electromagnetic waves in graphene-coated partially filled chiroplasma cylindrical waveguide. *Plasmonics* 1–11

**Publisher's Note** Springer Nature remains neutral with regard to jurisdictional claims in published maps and institutional affiliations.

Springer Nature or its licensor (e.g. a society or other partner) holds exclusive rights to this article under a publishing agreement with the author(s) or other rightsholder(s); author self-archiving of the accepted manuscript version of this article is solely governed by the terms of such publishing agreement and applicable law.